MSc Thesis
Utrecht, June 2018

Universiteit Utrecht

Quartz dissolution at mica-quartz interfaces due to surface potential effects

Author: H.L. Burgsteijn[1]
Supervisors: C.J. Spiers[1], S.J.T Hangx[1], H.E. King[1]
1 Faculty of Geosciences, Universiteit Utrecht

---

1 Abstract

Time-dependent compaction creep processes play an important role in compaction behaviour of clastic sediments in subsiding basin settings. We performed dissolution experiments on quartz grains in contact with either quartz (similar surface contact) or in contact with mica (dissimilar surface contact) under different amounts of applied normal stress over the grain contacts, to investigate the effect a dissimilar surface has on the dissolution velocity under in-situ stresses. We qualitatively compared dissolution under different stresses and with varying concentrations of dissolved Calcium (Ca^{2+} cations). The surfaces of these grains were imaged using an atomic force microscope (AFM) to visualize the dissolution features (e.g. etch pits) and measure the depth of these features to approximate dissolution rates. The experiments were inconclusive in showing quantitative results for the dissolution rates, but showed qualitative results on the grain contacts in the form of dissolution features after the month long duration of the experiment that were not present on the grain contacts before the experiments started. The theoretical model contains both the effects from grain contact stress and the effect of dissimilar mineral surfaces on dissolution velocities. The dissolution velocity increases both with the difference in surface potential between the surfaces and an increased stress across the grain boundary. The lower the effective surface potential of the dissimilar surface in contact with the quartz grain is, the higher the dissolution velocity will be. Resulting in a factor ≈ 2 increase in dissolution velocity for a quartz-mica contact compared to a quartz-quartz contact.

2 Introduction

Time-dependent compaction creep processes play an important role in controlling the porosity and permeability evolution of clastic sediments deposited in subsiding basin settings. In addition to brittle creep processes such as microcracking, stress-enhanced dissolution (i.e. pressure solution) at wetted grain contacts may also play a role. Pressure solution is a three step serial process consisting of dissolution of material at the grain contact, diffusion through the grain boundary fluid and precipitation on pore walls. The overall rate of pressure solution is controlled by the slowest of these processes, which for many solids are the interface kinetics. There is a negative correlation between porosity in clastic sediments and the clay content of those rocks, due to increased cementation of the rock as a result of pressure solution (Heald 1956) (Tada and Siever 1989). This relation can be seen in figure 1. This is evidence for an increase in pressure solution processes due to mica presence in nature. According to Heald (1956) clay promotes pressure solution in some rocks but is not required for the process.

Microstructural observations of sandstones have shown that certain minerals (micas, zircon, ilmenite) in contact with quartz grains are able to enhance pressure solution in the latter (Kristiansen et al. 2011) (Israelachvili et al. 2013) (Greene et al. 2009). Figures 2A and 2B, show two examples of enhanced pressured solution in

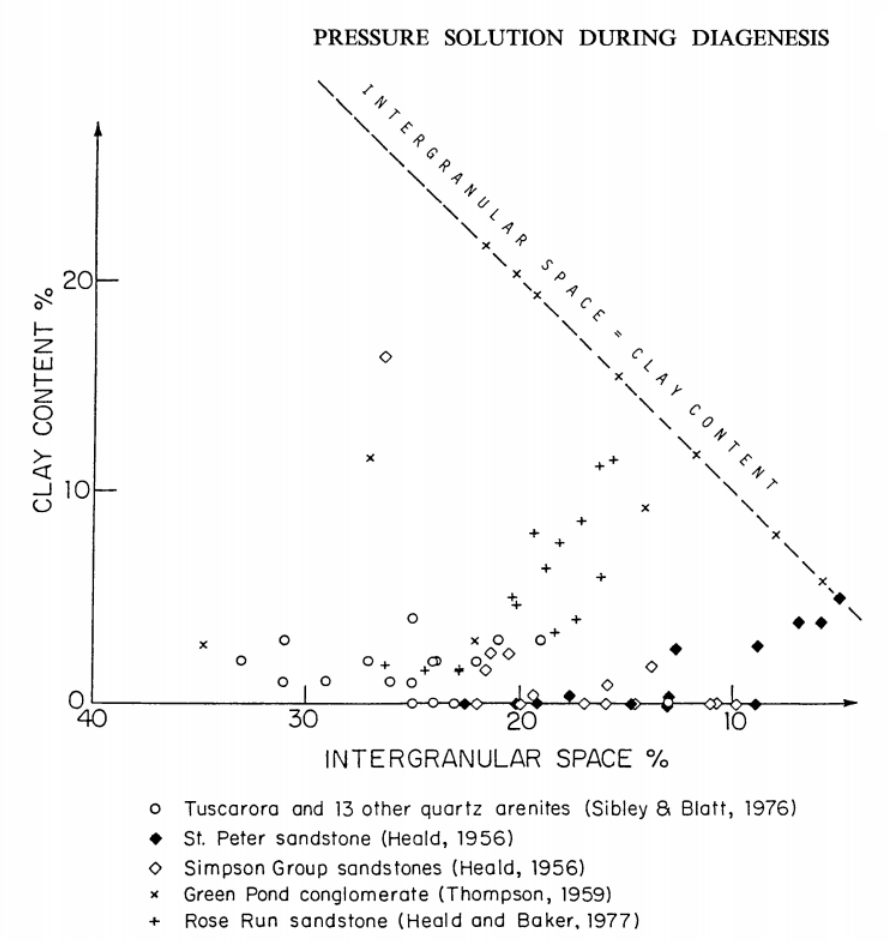

Figure 1: *Tada and Siever (1989) Variations of minus cement porosity with clay content in various rock samples from different authors. Sibley and Blatt (1976) Thomson (1959) Heald and Baker (1977) Heald (1956)*

natural samples of sandstones with micas present, while 2C shows almost no evidence of pressure solution in a pure quartz sandstone that is found 2 inches above the sample shown in 2B. Previous studies, performed at atmospheric conditions and very low applied load, have observed that this is due to enhancement of the quartz dissolution rate, related to the overlapping of the electric double-layers when two dissimilar surfaces are in sufficiently close proximity and the surface potential of the two surfaces change (Kristiansen et al. 2011) (Israelachvili et al. 2013) (Greene et al. 2009).

In the case of a mica-quartz interface, the quartz surface potential will become more negative when brought in contact with mica. This results in the attraction of more cations from the solution (e.g. Mg^{2+}, Ca^{2+} or Na^{+}) to the quartz surface. According to Dove and Nix (1997) increases in cation concentration near quartz surfaces increases the dissolution rate of the quartz, cations that increase the dissolution rates are in order of increasing effectiveness: $Mg^{2+} < Ca^{2+} \approx Li^{+} \approx Na^{+} \approx K^{+} < Ba^{2+}$. However another cation (Al^{3+}) can decrease the dissolution rate of quartz. Pressure solution in quartz aggregates is dissolution controlled for porosities down to 15% (Niemeijer and Spiers 2002), this means an increase in dissolution rate due to the presence of mica or clays at the quartz contacts in combination with the presence of certain cations in the interstitial water can enhance the pressure solution process in a naturally occurring sandstone.

The main problem with research by Kristiansen et al. (2011), Israelachvili et al. (2013) and Greene et al. (2009) is that it is done at low pressures of 3-5 atmosphere (0.3-0.5 MPa), while under in-situ reservoir conditions

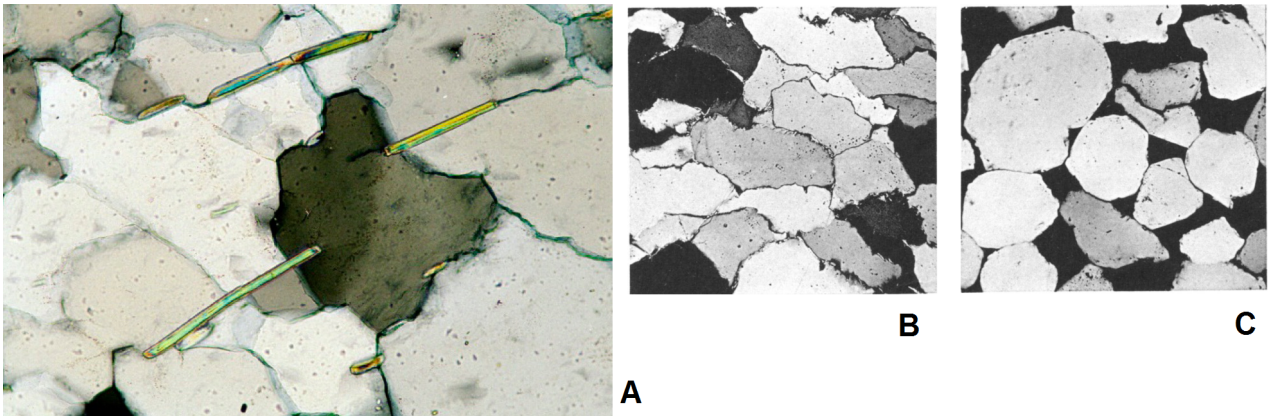

Figure 2: *Three different photomicrographs taken with crossed nicols polarizers microscopes of natural examples of pressure solution enhanced by the presence of mica and clays. A) 0.5 mm long soft mica flakes penetrating into hard quartz. (sample from Appalachian mountain area) Israelachvili et al. (2013) photomicrograph by J. R. Boles, UCSB Earth sciences collection.) B) Highly dissolved clay-rich sandstone with sutured contacts and low porosity in addition to elongation of the grains parallel to the (horizontal) bedding. (Sample from St. Charles County, Missouri) Heald (1956) C) Clay-free sandstone collected 2 inches above sample shown in B showing almost no pore space reduction.*

contact stresses can be three orders of magnitude higher. The goal of this research is to develop a model that incorporates the findings of previously mentioned researchers with more conventional pressure solution theories based on potential differences due to grain contact stresses. And if the surface potential effects resulting from mica-quartz contacts are still present when a high contact stress is applied, simulating in-situ reservoir conditions. The results can form a basis to understand why and how clay particles at grain contacts in sandstones enhance the rate of pressure solution in siliclastic rocks.

3 Methods

To investigate the effect of a quartz-mica boundary on the dissolution of the quartz grain, both a model for the kinetics will be developed and experiments will be conducted on quartz-mica interfaces and quartz-quartz interfaces.

3.1 Experimental setup

The main setup consists of three quartz grains that are glued to a glass plate in a triangular shape. On top of this triangle a circular slice of either mica or the 1010-surface of quartz is placed on top of which additional weight can be placed. This setup is then placed in a solution with a pH of 9, varying weights placed on top of the triangle to simulate normal stress across the grain contact and varying Ca^{2+} concentrations for a month due to low dissolution rates at room temperature, the calcium concentration for the various experiments can be seen in table 1 in addition to the amount of induced contact stress as a result of the added weights. The weights were made from steel and wrapped in non-soluble plastics to avoid oxidation of the steel and contamination of the solution.

To determine the mass of the steel weights we used the next 3 formulas to calculate a (the radius of the contact circle between two grains) assuming there is an idealized Hertzian contact Brzesowsky et al. (2011) where substituting formula [2] into [1] gives formula [3]:

$$a^3 = \frac{3FR}{4E^*} = \frac{3FR}{4}\left[\frac{(1-v_1^2)}{E_1} + \frac{(1-v_2^2)}{E_2}\right] \quad [1]$$

$$\sigma = \frac{3F}{2\pi a^2} \text{ [2]}$$

$$a = \frac{\sigma\pi R}{2}E^* \text{ [3]}$$

Where for quartz the Poisson ratio and the Young's modulus are $v_1 = 0.077$ and $E_1 = 95.68$GPa respectively and for mica $v_2 = 0.3$ and $E_2 = 6$GPa (Simmons and Wang 1971). This leaves two unknowns in formula [3], σ which is the stress at the grain contact and a the contact radius. When the contact stress is set at 0.5 MPa the resulting contact radius is $6.36 \cdot 10^{-9}$m per quartz grain and for a contact stress of 100 MPa, $a = 6.36 \cdot 10^{-6}$m. Then using formula [1] which has two unknowns the applied force (F) and the contact radius (a). Using the contact radius a, resulting from a contact stress of 100 MPa we get a resultant force required that is equal to 7.78g divided between three grains. Each weight used in the 100 MPa experiments was 7.8g. The weight required for the 0.5 MPa experiments was approximated by the weight of the circular slice of either mica or quartz (≤ 0.05g) on top of the three grains.

Calcium chloride dihydrate is used to increase the Ca^{2+} molarity of the solutions and sodium hydroxide is used to increase the pH to 9 using a pH-meter. The amount of sodium added to achieve the required pH is negligible compared to the calcium and since the effect of sodium and calcium on quartz dissolution is similar Dove and Nix (1997), the effect on dissolution rate from the cations will depend on the calcium concentration. The quartz grains that are used are selected from sieved batch (300-500 μm) of Ottawa quartz sand. These grains are then photographed from the side at two perpendicular angles, and the radius of curvature is measured for each of the directions see figure 5. The average radius of curvature per grain can be found in figure 3, the average radius of curvature for all grains is 289 μm. The pH of 9 is chosen due to the effective surface potentials of both quartz and mica at that pH, in figure 4 the effective surface potentials of mica and quartz are plotted as a function of the pH. The figure shows that mica has a lower surface potential than quartz for a pH ≥ 5, we have chosen for a pH of 9 due to relative stability of difference in effective surface potential in that pH range Kristiansen et al. (2011).

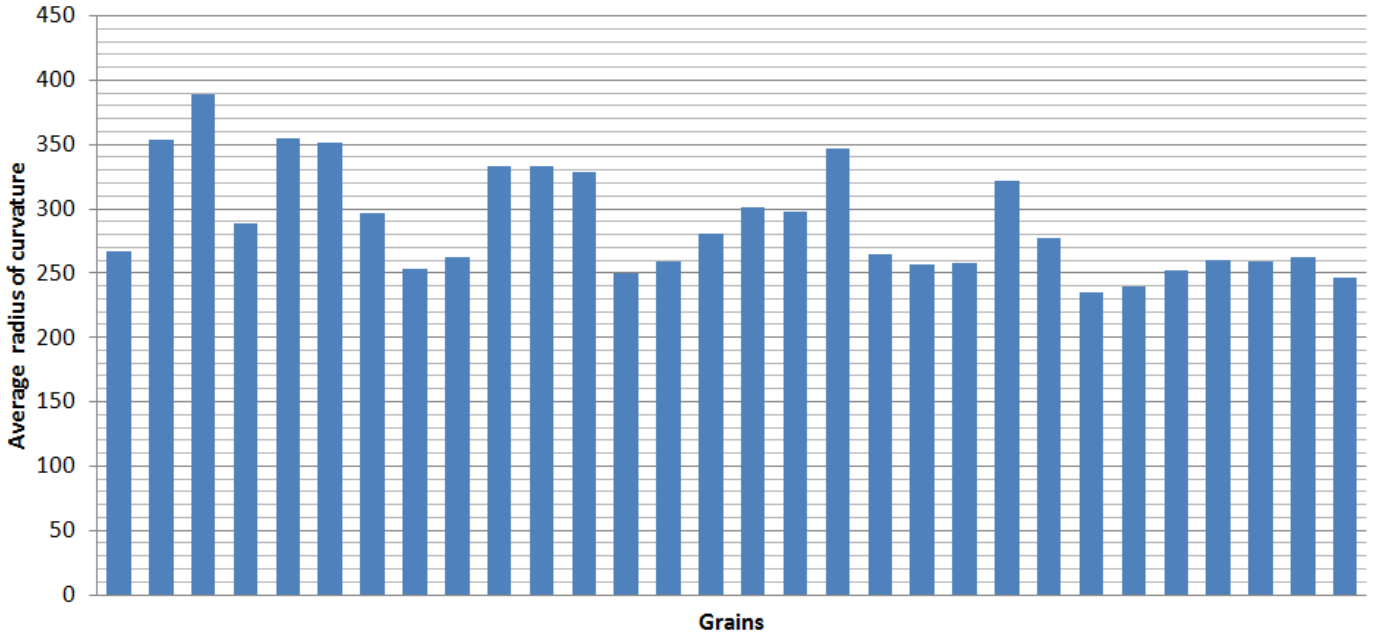

Figure 3: *Measured average radius of curvature in micrometers from two perpendicular angles. Each bar represents one of in total 30 grains.*

The 10 experimental setups seen in table 1 can be divided into four main groups, quartz-quartz grain con-

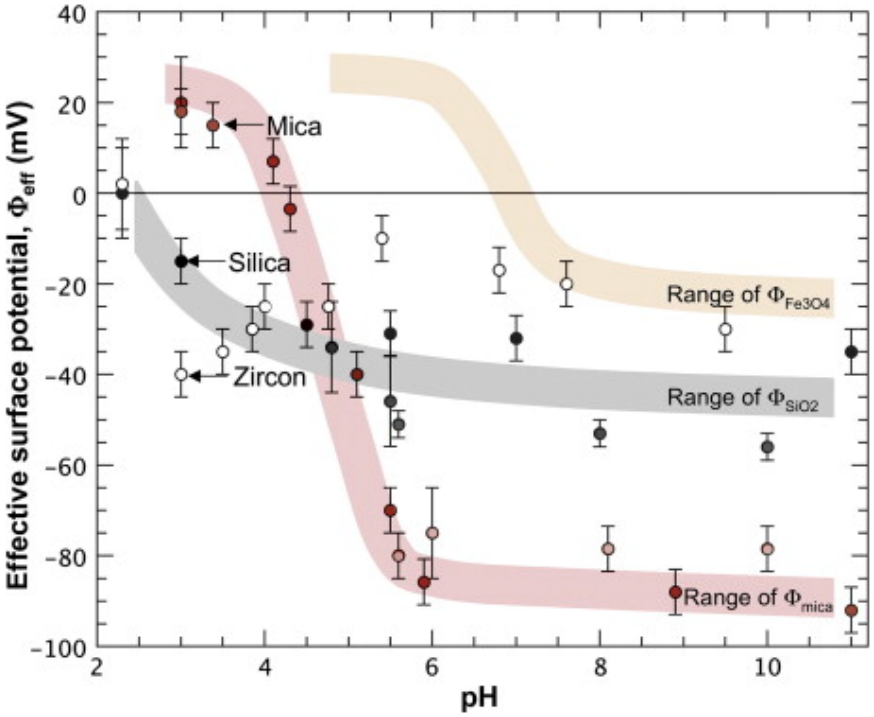

Figure 4: *Surface potential relations of common minerals as a function of pH measured with AFM, Kristiansen et al. (2011).*

Contact: Mica-Quartz			Quartz-Quartz		
Experiment no.	Ca^{2+} (mM)	Stress (MPa)	Experiment no.	Ca^{2+} (mM)	Stress (MPa)
1	0	0.5	6	0	0.5
2	5	0.5	7	5	0.5
3	30	0.5	8	30	0.5
4	0	100	9	0	100
5	30	100	10	30	100

Table 1: *Experimental setup values for all 10 experimental setups.*

tacts and quartz-mica contacts both of these groups are tested with and without a stress. Within each of these groups the cation concentration is varied from 0-30 mM. 50 mM Ca^{2+} concentration leads to saturation of the quartz surface sites for cations and adding more cations to the solution will not increase the dissolution rate further Dove et al. (2005). At the mica-quartz contacts the quartz grains should attract more Ca^{2+} cations by a factor of 50 according to Kristiansen et al. (2011) at a pH of 9, due to the negatively charged mica lowering the surface potential of the quartz and resulting in increased attraction of cations to the surface. This means that the effective Ca^{2+} cation concentration at the quartz surface for experiment 2 is $5 \cdot 50 = 250$mM and for experiments 3 and 5 the effective concentration is $30 \cdot 50 = 1500$mM. Both these values (250-1500mM) far exceed the saturation of the quartz surface, which means that if Kristiansen et al. (2011) is correct the results of experiments 2 and 3 should be similar. For experiments 7 and 8 at the quartz-quartz contacts the quartz surface concentration of Ca^{2+} should not be saturated, since there is no multiplication due to extra attraction. This means that there should be differences in the amount of dissolution between experiments 7 and 8. Experiments 4,5,9 and 10 have a normal stress of 100 MPa at the grain contact and should show an increase in dissolution rate due to gradients in the chemical potential between the grain contact and the grain boundary not in contact. Experiments 1,4,6 and 8 are performed without cations in the solution and thus should have the slower dissolution rates in addition to not showing a difference between the mica-quartz and quartz-quartz experiments, since there are no cations that the quartz surface can attract due to the drop in surface potential

Figure 5: *Photograph from the side of a sample, used for calculating the radius of curvature.*

of the quartz grain caused by contact with mica.

Previous to these 10 experimental setups another 10 similar experiments where run. The data from these experiments where a stress of 100 MPa was applied are unusable due to oxidation of the steel weights during the month-long duration of the experiments. This oxidation turned the colour of the bulk liquid orange and prompted the use of clear plastic coating on the weights in further experiments. In addition to the oxidation there were problems with the epoxy resin not holding some of the grains to the glass plate, leading to a loss of 6 of the remaining 18 grains not lost to oxidation. We decided to repeat all the experiments with plastic coated weights and cyanoacrylate adhesive in addition to changing the pH of the solution to 9 instead of the originally used 3. This change in pH allowed for a more stable experiment where small pH changes over the course of the experiments did not change the relative effective surface potential of the mica and quartz, see figure 4.

3.2 Height Measurements

The atomic force microscope (AFM) Binnig et al. (1986) is used to inspect the surface of the quartz grains before and after the experiments. The AFM was used in contact mode with a tip velocity of 14.8 $\mu m/s$ at 384 samples per line, 384 lines and a scan rate of 2.47 Hz. The need to be able to look at the samples before and after the dissolution made it impossible to use a scanning electron microscope (SEM), since that would require coating the grains with a conductive material prior to the dissolution which might influence the experiments. A height scale for the measurements is chosen after the measurement is done due to major difference in scale between the sample surfaces, a single constant scale would hide a lot of information due to it not fitting the scale of the actual measurement. The top point of each grain is found using an optical microscope and then further investigated with the AFM, since that is the part of the grain in contact with the mica surface in addition to being the point that experiences stress, therefore dissolution should be at a maximum at this point. Each of the measurements done with the AFM have a surface of 3 by 3 μm and 10 measurements are done for each grain top (30 for each experimental setup), both before and after the experiments. Dove et al. (2005) Shows examples of etch pits found at these scales on dissolved quartz surfaces. The top point of the grain is where dissolution features such as etch- or dissolution-pits are expected when the experiments are completed. The depth of these pits and overall rounding or smoothing of the grain was used to determine the amount of dissolution qualitatively and gives an ability to compare the dissolution rates of the different experimental setups seen in table 1. In addition to the qualitative analysis a roughness analyses is also done $R_q = \sqrt{\frac{1}{n}\sum_{i=1}^{n} y_i^2}$ (root mean square roughness) and $R_a = \frac{1}{n}\sum_{i=1}^{n} \mid y_i \mid$ the arithmetic average of absolute values are determined for each AFM image. The five criteria that are measured for each image are: depth of larger etch pits, quantity of etch pits, overall roughness (R_a and R_q) and the roughness on larger asperities on the surface.

4 Hypotheses

This section will contain hypotheses for relative dissolution velocities of the 10 experiments mentioned in table 1 and explanation on why exactly these experimental setups were chosen. Comparing experiments 3 and 8 could show the effect of the decreased surface potential of quartz due to contact with mica in experiment 3. If it is correct that due to the lower quartz surface potential in experiment 3 additional cations are attracted to the quartz surface it should result in a higher dissolution velocity of the quartz grain in experiment 3 compared to experiment 8. There should be no differences in dissolution velocity between experiment 1 and 6, since the mechanism by which the mica-quartz surface would increase dissolution velocity requires there to be cations in the bulk solution. To investigate the effect of the cation saturation of the quartz surface we look at experiment 2 and 3. In these experiments there should be a up to a factor 50 higher concentration of cations near the quartz surface than in the bulk fluid due to the influence of the lower surface potential of the mica. Meaning both of these experiments easily reach the quartz surface saturation of cations of 50 mM and there should be no difference in dissolution velocities between the experiments due to this saturation. This is different for experiment 7 and 8, where the cation concentration in the bulk fluid should be equal to the quartz concentration at the quartz surface. Thus the dissolution velocity should be higher in experiment 8 compared to experiment 7 due to a higher concentration of cations in the bulk fluid and both having a undersaturated quartz surface. Comparing experiment 1 and 4 and 6 and 9 respectively would show the effect of increased quartz dissolution in the grain contact driven by grain contact stress in both quartz-quartz and quartz-mica contacts. Due to the absence of cations in the solution the presence of mica should have no effect on the dissolution velocity of quartz so the velocity of the dissolving grain contact in experiments 4 and 9 should be similar, just like experiment 1 and 6 should show similar dissolution rates although both 4 and 9 should show higher dissolution rates than experiments 1 and 6 due to a higher grain contact stress in experiments 4 and 9. Comparing experiment 5 with 10 would give insight into the ability of grain contact stress to (partially) negate the effect of the decreased surface potential of the quartz surface due to mica presence in experiment 5 has. According to our current theoretical model the dissolution velocity should increase in experiment 5 compared to 3 and 10, since both the enhancing effect of mica presence and increased grain contact stress are simultaneously present in experiment 5.

5 Results

5.1 Model

The maximum dissolution velocity of quartz found in Kristiansen et al. (2011) of $\Delta h = 5$ Å per hour or $1.4 \cdot 10^{-13}$ meters per second, Δh represents the height retreat of a quartz sheet in proximity to a electrode surface with a negative electrochemical potential. From this height retreat we can determine the area of the grain contact using the geometry of a spherical cap as seen in figure 6. This maximum dissolution velocity results in a contact area radius of $a = \sqrt{2r\Delta h - \Delta h^2} = 13.4 \mu m$ for a flattened spherical grain after a months time when Δh is 360nm after a month, where r is the original radius of the grain (250 μm), for the full development of the area radius during the whole month see figure 7. The new flattened contact area increases over the duration of the experiment due to the dissolution of the non-flattened grain. This has two implications if the rate is correct and can be replicated in experiments. The first implication is that such a significant change in contact area should be visible with an optical microscope and that the surface topography will be heavily changed due to the dissolution process and all pre-existing surface features are replaced with new features such as etch-pits. The second implication is that the contact stress will decrease over the course of the experiment, since the applied force remains the same while the contact area increases. This effect can be seen in figure 8, where the contact stress under a load of 2.5g decreases from 1300 MPa to 43 Mpa in a 30 days time for an average contact stress of 103 MPa for the last 28 days. At the start of the experiment the quartz grain will be more spherical and so it will closely resemble a Hertzian contact described in equations [1], [2] and [3]. This means the normal stress at the start will be 100 MPa due to the 7.8g weights and the Hertzian contact, while slowly becoming more like a spherical cap instead of a spherical grain, which means that the effect seen in figure 8 takes over. This model would prevent stresses higher than 100 MPa at the start of the experiment. The presence of smaller asperities on the surface

of the grains can increase the contact stress at the start of the experiment due to the contact radius decreasing for the Hertzian contact, although measurements seen in 5 show no major outliers in terms of contact radius.

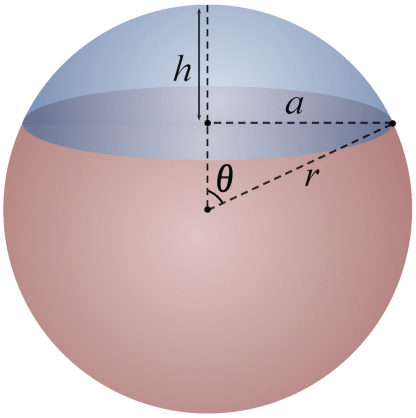

Figure 6: *Schematic representation of a spherical cap*

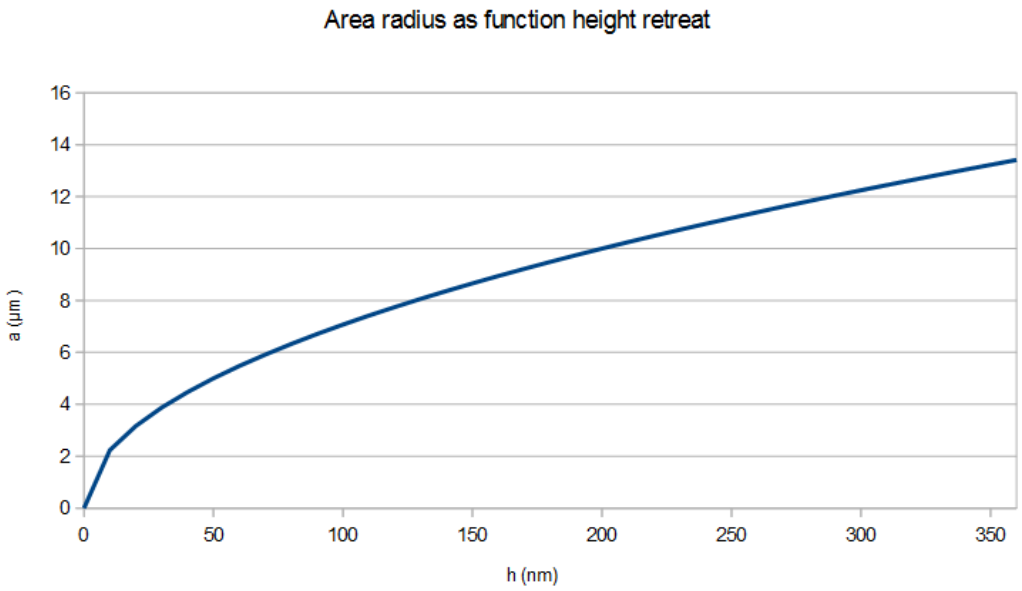

Figure 7: *The increase in area radius in µm of the spherical grain cap during a height retreat of 360 nm. Where the radius of the sphere is 250 µm*

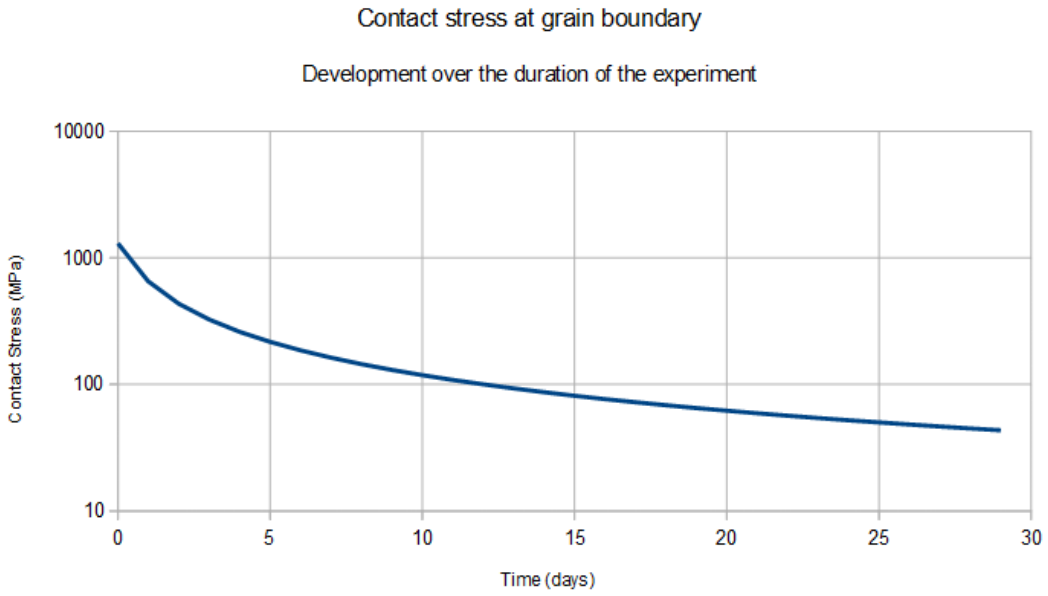

Figure 8: *Development of the normal stress on the grain contact over the course of the month-long experiments.*

To arrive at a model for compaction creep enhanced by the effect of surface potential, we first need a model for regular compaction creep. Compaction creep is driven by dissolution for porosities down to 15% for pure quartz Niemeijer et al. (2002). In the rest of this model we will assume that the processes involved are dissolution controlled and that both diffusion and precipitation are not limiting. The model from Pluymakers and Spiers (2015) is used, they derived a model for dissolution-controlled compaction creep.

$$V_c = I_s \left[exp\left(\frac{\sigma_n \Omega}{RT} \frac{Z}{F} \frac{q}{q - 2\phi} \right) - 1 \right] \text{ [4]}$$

Where V_c is the uniform velocity of a dissolving grain contact surfaces in meters per second, assuming that the two dissolving grain contacts remain flat. This velocity depends on the σ_n (average normal stress across grain boundary in Pa), Ω (molar volume of the solid phase, 2.269 $m^3 mol^{-1}$ for quartz), T (absolute temperature, 293.2 K for room temperature), Z (grain coordination number, 6 for simple cubic pack of grains), F (grain shape factor, π for spherical grains), q (twice maximum porosity of spherical grain aggregate with grains that are just touching), ϕ (porosity of grain aggregate) for quartz at 100MPa ϕ=0.2 and $q = 2\phi_0 = 2 \cdot 0.5 = 1$ for the maximum porosity Robinson and Gluyas (1992). The three most important terms are the pre-factor I_s which is the dissolution rate constant in ms^1, the temperature and the average normal stress. This shows that the model is both temperature and stress dependent. To add the effect of surface potential influence from the nearby mica grain we are going to change the I_s pre-factor.

$$I_s = \alpha k_+ \Omega \text{ [5]}$$

Where α is a factor allowing for the grain boundary structure on grain boundary dissolution rate ($\alpha \approx 0.9$ van Noort and Spiers (2009), which we assume remain unchanged. k_+ Is the geochemical dissolution constant for an unstressed solid in $molm^{-2}s^{-1}$ at a reference pressure P_f. This is where we assume the mica presence comes into effect on the model. The next equation [6] is from Rimstidt (2015) and shows a k_+ value for sodium catalyzed quartz dissolution. Where m_{na^+} is the sodium concentration and a_{H^+} is the hydrogen ion activity. In our experiments we use Ca^{2+} instead of Na^+, which are both salts that increase quartz dissolution rates at a similar quantities (Dove and Nix (1997). We used a_{H^+} is $1 \cdot 10^{-9}$ which equals a pH of 9, a temperature of 293.2 K to represent room temperature and R is the gas constant.

$$k_+ = 0.646 \left(10^{\frac{-74800}{2.303R} \frac{1}{T}} \right) + 6.64 \left(10^{\frac{88000}{2.303R} \frac{1}{T}} \right) \left(\frac{m_{Na^+}^{0.331}}{a_{H^+}^{0.441}} \right) \text{ [6]}$$

The link to the mica presence comes from the decrease in surface potential of the quartz which will increase the cation concentration near the quartz surface Greene et al. (2009). The next equation [7] shows the m_{na^+} (concentration of the cation near the quartz surface) and $m_{na^+}^{inf}$ the cation concentration in the bulk solution and an exponential factor that contains the change in surface potential $\Delta\psi_0$ of the quartz contact. A decrease of 50 mV of the surface potential will increase the cation concentration by a factor 52 for calcium with a z-value of 2, figure 9 shows the relation between this factor and the decrease in surface potential. Which will in turn increase the k^+ value, which positively affects the V_c from the original model, figure 10 shows the relation of k^+ and $\Delta\psi_0$. So a decrease in surface potential due to the contact with a mica grain will increase the dissolution velocity of quartz. There is a maximum m_{na^+} of 50mM included to represent the saturation of the quartz surface according to Dove et al. (2005) after which additional cations added to the bulk solution will not affect the cation concentration at the quartz surface. k_b is the Boltzmann constant ($1.38064852 \cdot 10^{-23} JK^{-1}$) and e is the elementary charge ($1.602176634 \cdot 10^{-19}$ C)

$$m_{na^+} = m_{na^+}^{inf} \cdot exp\left(\frac{-ze\Delta\psi_0}{k_bT}\right) \text{ with } m_{na^+} \leq 50mM[7]$$

Combined these formulas give an equation that depends on both stress and geochemical potential changes. Where an increase in stress increases the dissolution velocity and a decrease in the surface potential of the quartz grain will increase the dissolution velocity. Figures 11, 12 and 13 show velocities of dissolving grain contact surfaces, with V_c on a logarithmic scale. In figure 11 the line of 30 mM at 0mV has 6% lower values of V_c than the line of 5mM and 30mM at -25mV although they appear to be at similar values in the graph. In figure 10 the value of k_+ is constant for $m_{na^+}^{inf} = 0$ and show an exponential dependence on $\Delta\psi_0$ until $\Delta\psi_0 = -29mV$ and $\Delta\psi_0 = -7mV$ for $m_{na^+}^{inf} = 5mM$ and $m_{na^+}^{inf} = 30mM$ respectively, after which $m_{na^+} \geq 50mM$ and as a result k_+ becomes a constant due to cation saturation of the quartz surface.

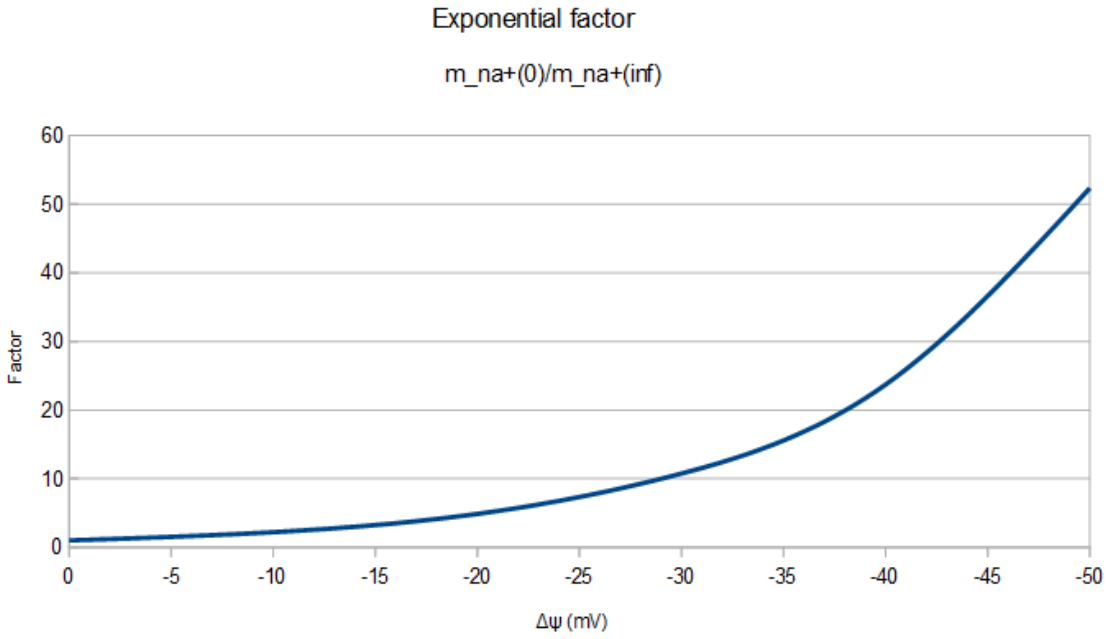

Figure 9: *Results from the model in equation [7], showing the exponential factor changing with the difference in surface potential between the two grain surfaces. The exponential factor is the relative increase in cation concentration near the grain surface compared to the bulk fluid, equal to the ratio of* $\frac{m_{na+}}{m_{na^+}^{inf}}$

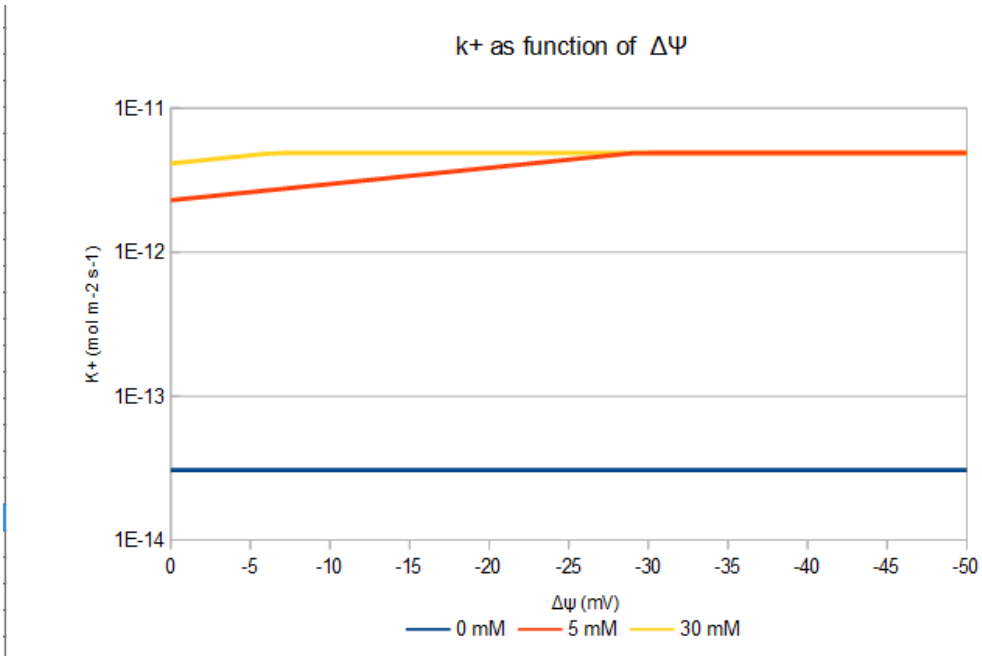

Figure 10: *Results from the model in equation [6], showing the dissolution flux for a changing difference in surface potential between the two grain surfaces at different Ca^{2+} (0, 5, 30)mM concentrations in the bulk liquid.*

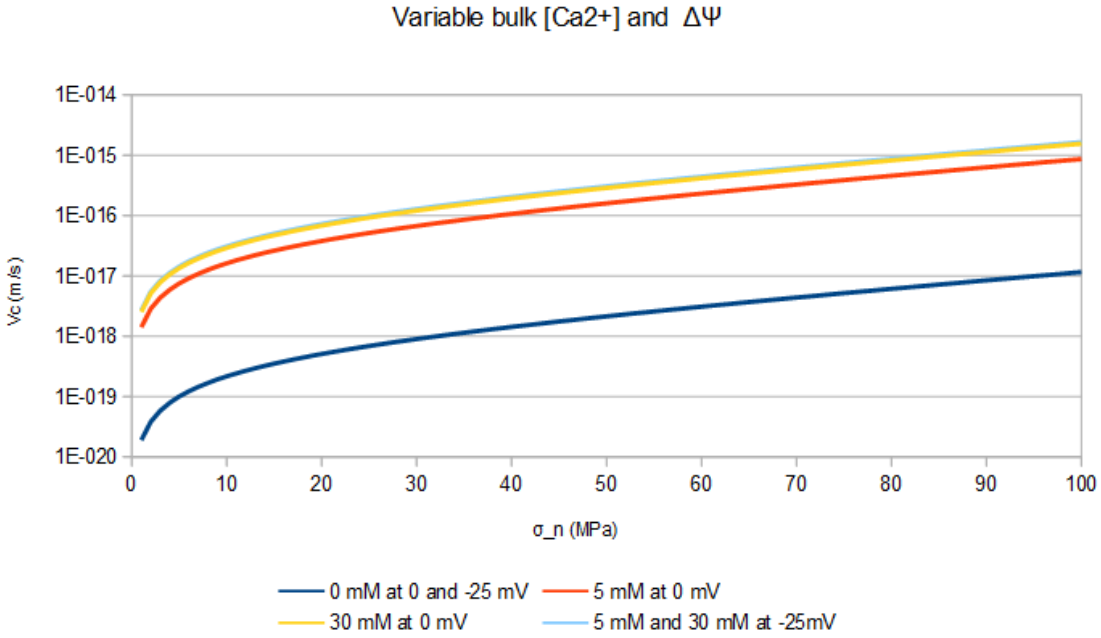

Figure 11: *Results from the model in equation [4], showing the velocity of a dissolving grain contact surface for a changing grain contact normal stress at different Ca^{2+} (0, 5, 30)mM concentrations in the bulk liquid. Where $\Delta\psi = -25mV$ or 0 mV for each of the concentrations which is analogue to a dissimilar surface contact between quartz and mica or a similar surface contact between quartz and quartz respectively.*

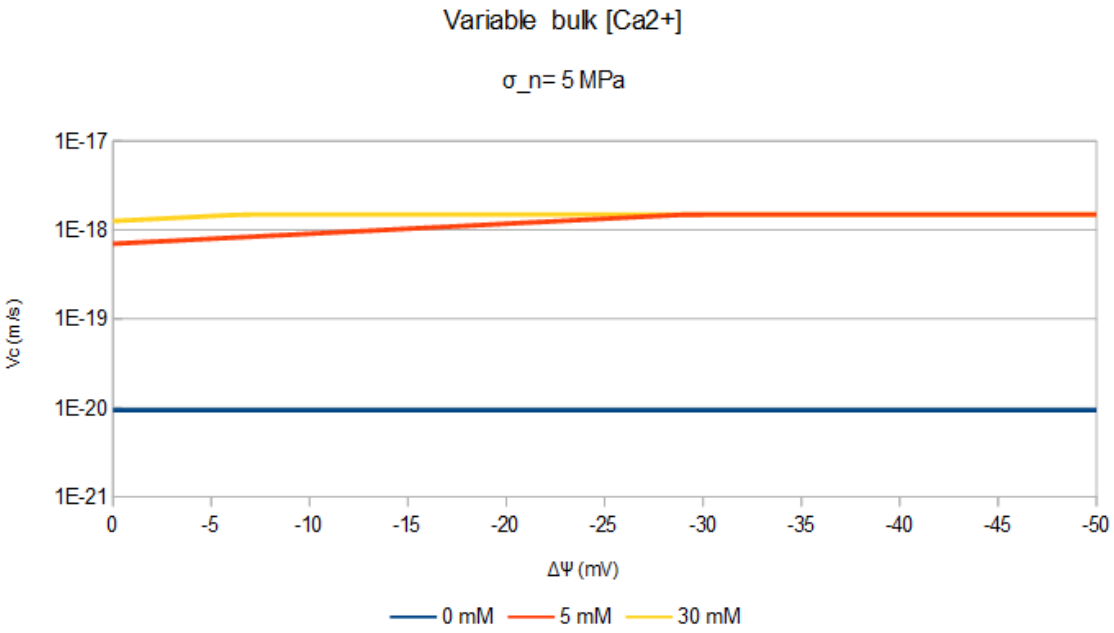

Figure 12: *Results from the model in equation [4], showing the velocity of a dissolving grain contact surface for a changing difference in surface potential between the two grain surfaces at different Ca^{2+} (0, 5, 30)mM concentrations in the bulk liquid. For a constant normal stress across the grain contact of 0.5 MPa.*

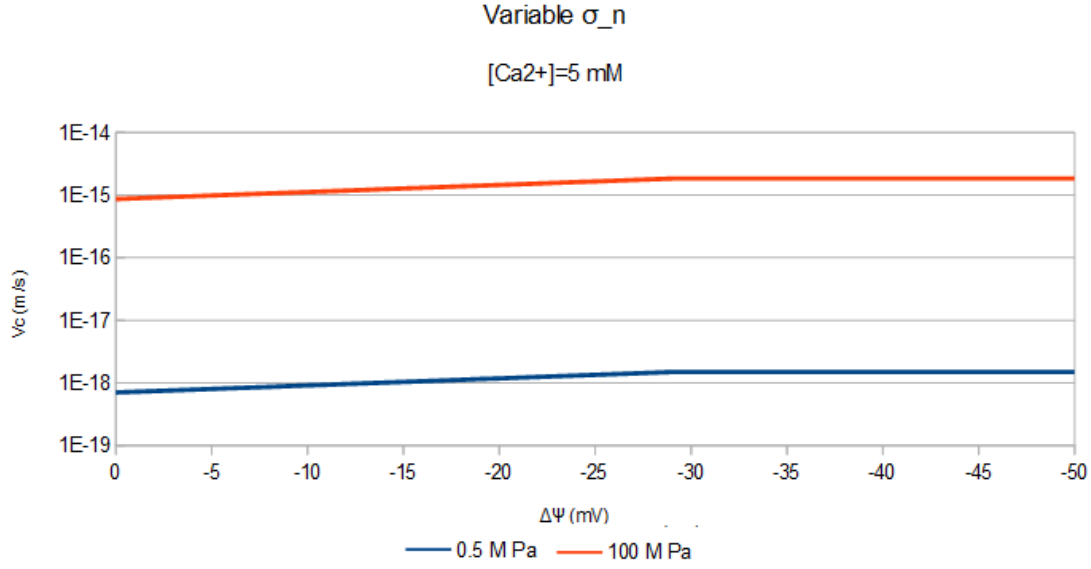

Figure 13: *Results from the model in equation [4], showing the velocity of a dissolving grain contact surface for a changing difference in surface potential between the two grain surfaces at different normal stresses across the grain contact 0.5 and 100 MPa. For a constant Ca^{2+} concentration of 5 mM.*

5.2 Experiments

The AFM images from before and after the experiments are all contained in the appendices A and B respectively, figure 14 shows two example images from experiment 8 (quartz-quartz, 30 mM Ca^{2+}, 0.5 MPa) after the experiment concluded and figure 17 shows two cross-sections through this sample. The two examples in figure 14 show the two main types of image collected with the AFM after the experiments, where A represents the small scale ($\leq 50nm$) and B represents the bigger scale ($\geq 100nm$). Similar results can be shown for experiment 3, seen in figure 15 this setup is very similar to experiment 8 seen in figure 14 with the difference being that the grain contact is dissimilar (mica-quartz). Figure 15 also shows these same main types of scales as well as the presence of etch pits in the $\leq 50nm$ scale in figure 15A. This means that dissolution of the sample has occurred, this can be seen in both figure14A and figure15A, but not on the bigger scale seen in figure 14B or the optical scale of figure 16. The five criteria that are measured for each image are: depth of etch pits, quantity of etch pits, overall roughness of the total AFM-image and the roughness on larger asperities.

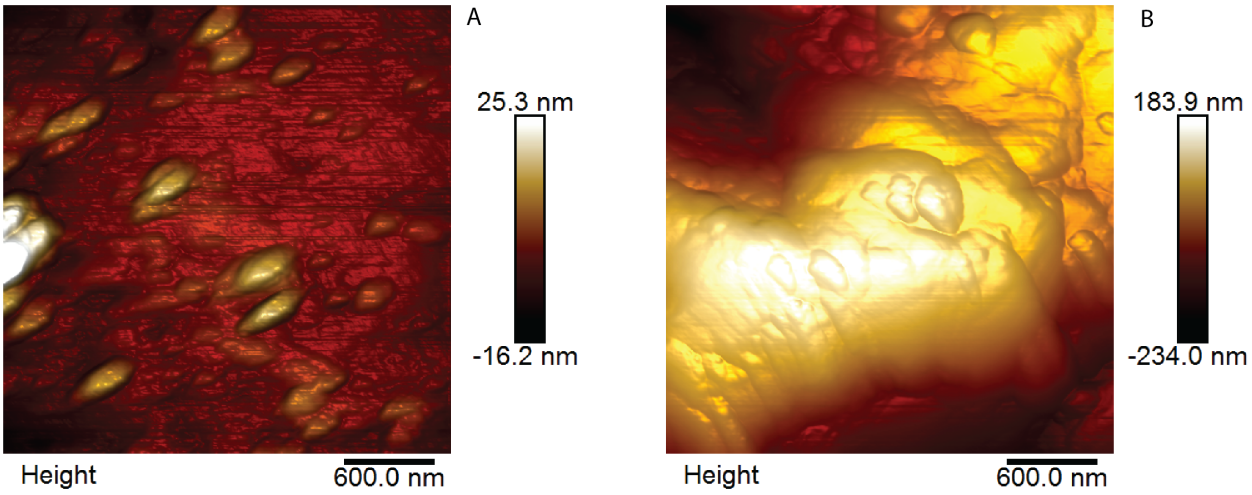

Figure 14: *AFM measurements of experiment 8 (quartz-quartz, 30 mM Ca^{2+}, 0.5 MPa) after the experiment concluded. A) Small height differences with etch pits visible B) Large height differences without visible dissolution features.*

First we look at the etch pits, which can be found in the small scale images, $\leq 50nm$ scale images are only present after the experiments are concluded, none of the AFM-images before the experiments show topography with scales below 250nm. This means that etch pits are only found after the experiments are concluded and no observations of etch pits are made prior to the experiments. On the small scale images the etch pits can be identified on the AFM-images of experiments 1,2,3,4,5,8,9 and 10 thus missing evidence of etch pits in experiment 6 and 7. The depth and size of the etch pits is measured as is shown in figure 17 using a profile through the etch pit. The etch pits in all experiments seem to have a maximum depth of 8nm and can be detected when they are deeper than 4nm. Most etch pits are 200nm in length and 100 nm in width. Figure 18 shows 5 additional etch pits in a single image of experiment 3. The steepness of the walls of the etch pits seem to mainly depend on the depth of the pit, with deeper pits having steeper edges. The typical angle for the etch pit walls is 8 degrees, which is seen in 4 of the 5 etch pits in figure 18. The etch pits are aligned similarly to protruding asperities in the same AFM-image and show a preferred orientation as can be seen in figure 18 with a long axis from the top left to the bottom right in this example. This can be explained by the small scale of the AFM-images that even though we are looking at quartz grain at this scale there is only one quartz crystal surface present in the image.

The overall roughness of each sample is mostly determined by the presence of larger scale features and the

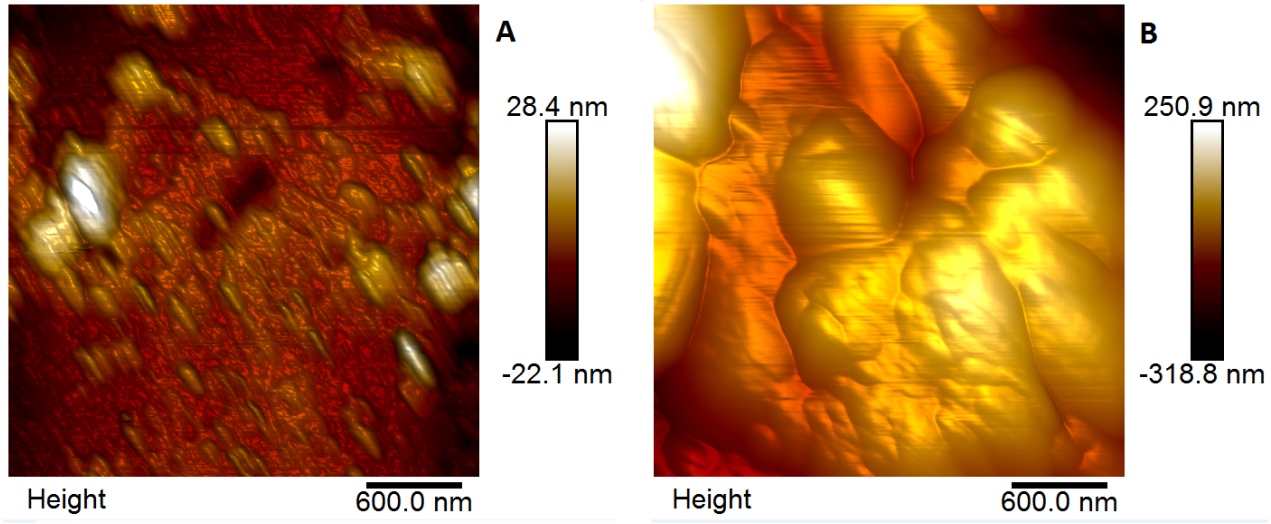

Figure 15: *AFM measurements of experiment 3 (mica-quartz, 30 mM Ca^{2+}, 0.5 MPa) after the experiment concluded. A) Small height differences with etch pits visible B) Large height differences without visible dissolution features.*

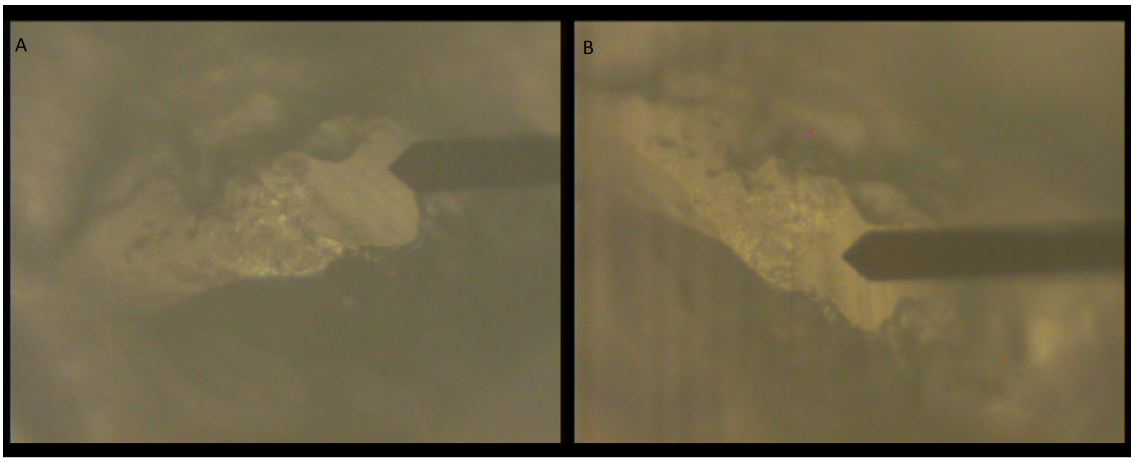

Figure 16: *Optical image of the top of the grain from experiment 5 (quartz-mica, 30 mM Ca^{2+}, 100 MPa). A) Before dissolution experiment B) After dissolution experiment*

overall scale of features of the sample. In figures 19 and 20 the average R_a (root mean square roughness) and R_q (the arithmetic average of absolute values of height) are shown for each experiment, both before and after. The average value is calculated by measuring the roughness for each individual AFM-image and averaging them per experimental setup. In addition to showing this average the graphs also show the average deviation of the roughness, which is the average of the absolute deviations for each individual AFM-image from the average roughness of the experiment (before and after separate) shown in the graph. These average deviations are more than a third of the average for most samples. The trends between before and after for both R_a and R_q are close to identical and show an increase in roughness for experiments 2 and 5, a decrease for experiments 1,8 and 10 and almost no change for experiments 3,4,6,7 and 9. The roughness on top and on the bottom of larger asperities such as the protruding asperities in figures 14B and 15B are very low with R_q and R_a values lower than 1nm, both before and after the experiments. Meaning these larger asperities are smooth, but the height differences between the tops, slopes and valleys result in overall roughness seen in figures 19 and 20.

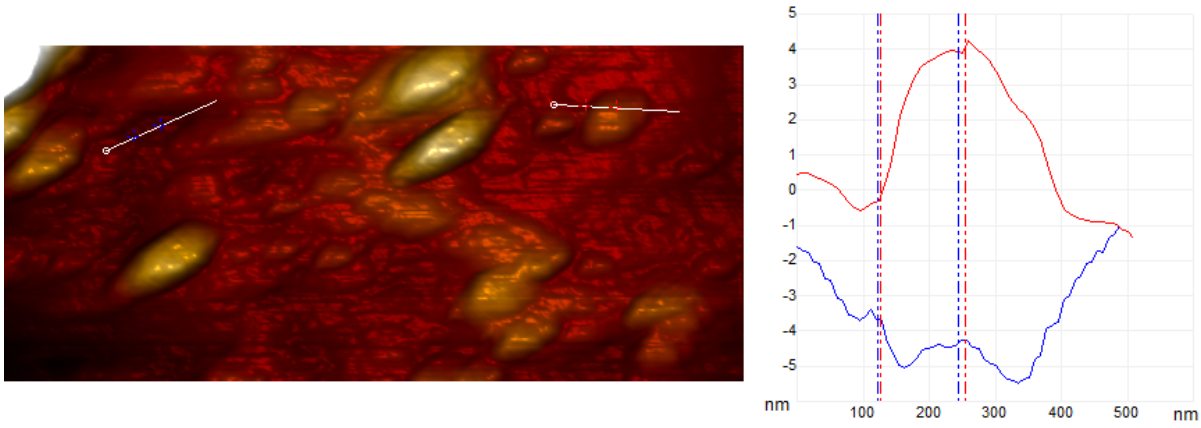

Figure 17: *AFM measurement of experiment 8 (quartz-quartz, 30 mM Ca^{2+}, 0.5 MPa). Corresponds to the same image as figure 14A and shows two different profiles through the topography, one through an etch pit (blue and on the left) and one through a lump (red and on the right)*

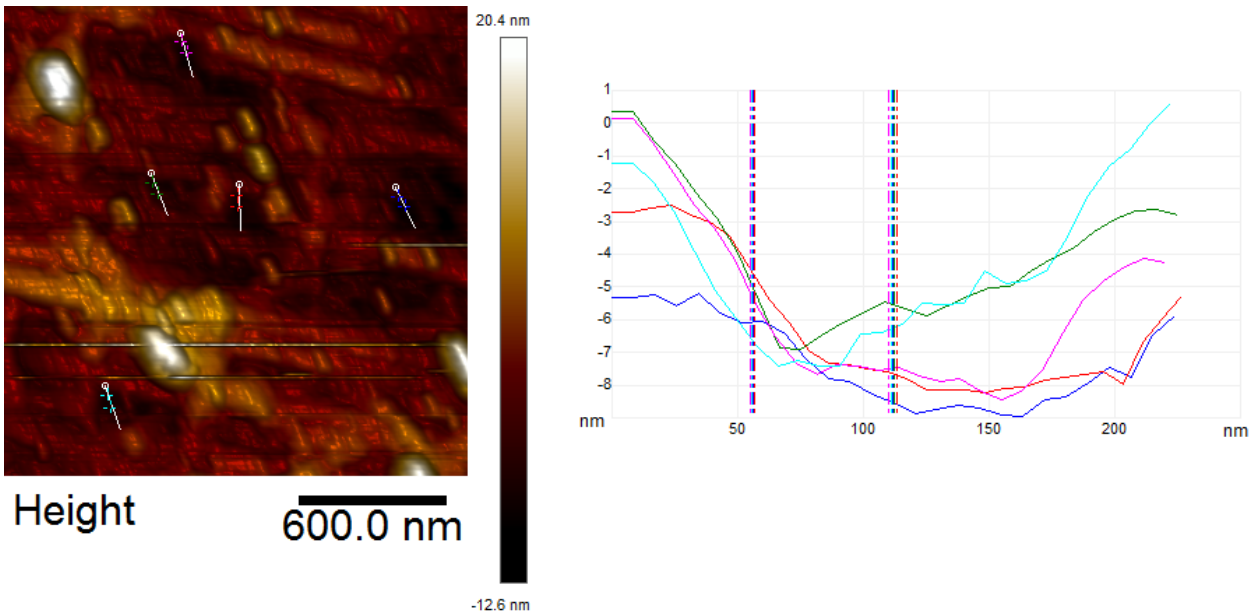

Figure 18: *AFM measurement of experiment 3 (quartz-mica, 30 mM Ca^{2+}, 0.5 MPa). It shows 5 different profiles through etch pits.*

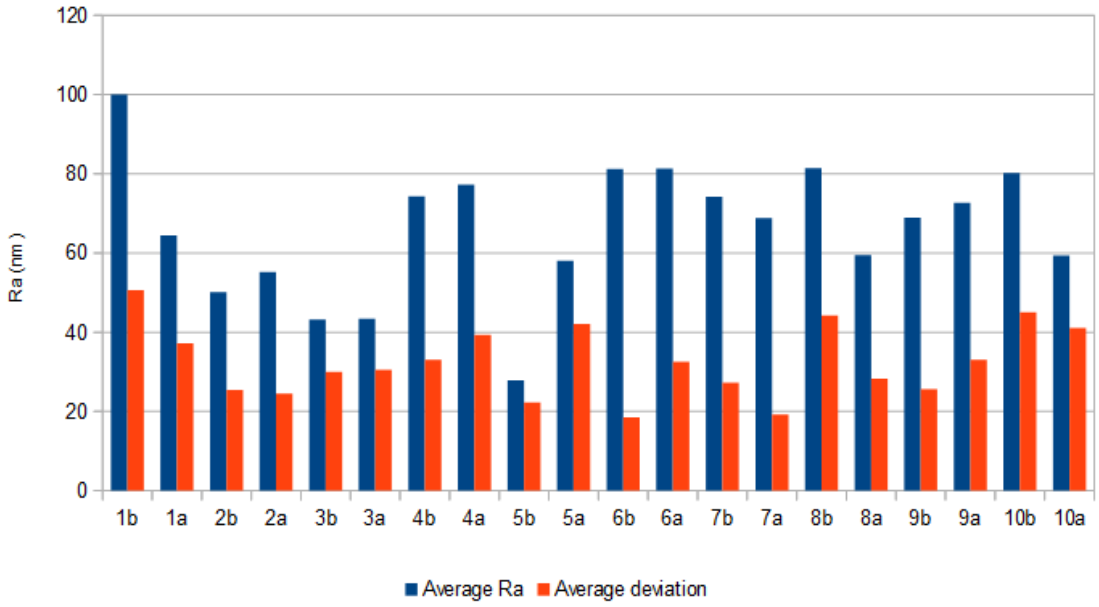

Figure 19: *Average R_a (the arithmetic average of absolute values of height) and the average deviation of R_a measurements for all experiments, before (b) and after (a). Number of experiments correspond to table 1.*

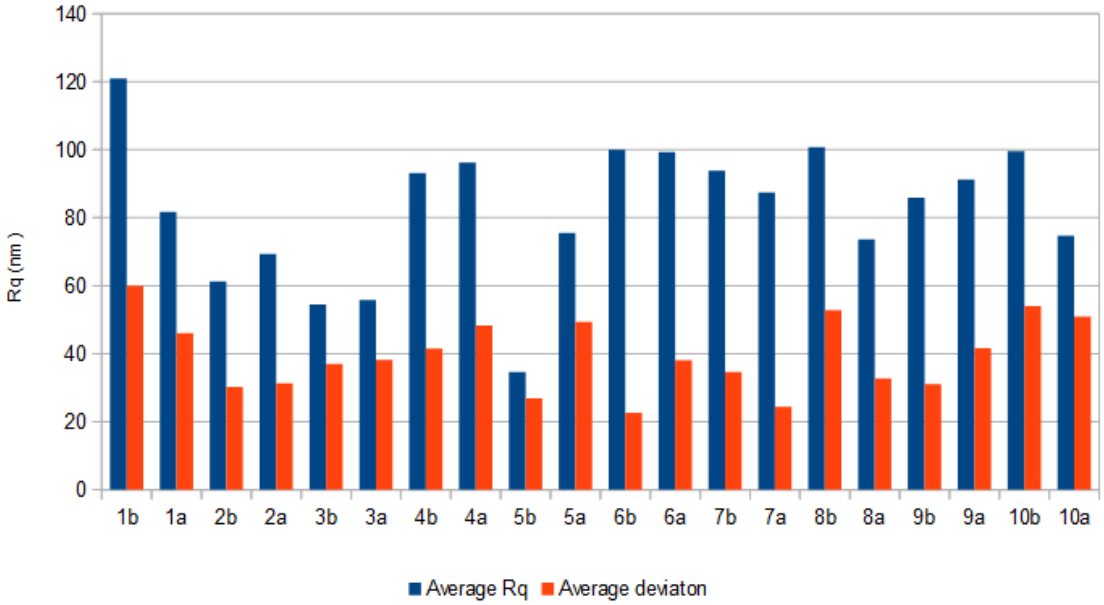

Figure 20: *Average R_q (root mean square roughness) and the average deviation of R_q measurements for all experiments, before (b) and after (a). Number of experiments correspond to table 1.*

6 Discussion

Our theoretical model shows both an influence of a contact between dissimilar surfaces and a contact stress can lead to an increase in velocity of the dissolving grain contact surface at the same time. In the current model the two different driving forces for dissolution (decreased surface potential of the quartz grain due to the mica contact and increased surface potential of the quartz grain contact due to an applied normal stress) seem to conflict with each other. These two driving forces do not necessarily have to conflict with each other if the increased surface potential due to applied normal stress across the grain contact is more local than the presence of mica. So that dissolution still occurs at points of high normal stress while precipitation occurs at points with low normal stress if both the point of high normal stress and the lower stressed grain boundary are in contact with the mica and have their surface potentials lowered accordingly. If only the grain boundary surface experiencing the high normal stress is in contact with the mica the two effects would (partially) negate each other. If only the grain boundary that is not experiencing the normal stress is in contact with the mica, it would result still result in a overall contribution to the driving force due to relatively lowering the surface potential of the non-stressed boundary compared to the stressed boundary. Although in this last case the additional effect on dissolution velocity due to the attraction of extra cations to the dissolving stressed grain boundary would not occur. Natural observations seem to contradict the negation of the effect of mica presence on dissolution velocity at the scale of a sandstone containing mica, since observations show a positive relation between mica presence and compaction rate of rocks Heald (1956).

The theoretical model shows a factor ≈ 1200 increase in velocity of the dissolving grain contact when increasing the normal stress across the grain contact from 0.5 MPa to 100 MPa. While decreasing the surface potential due to dissimilar mineral contact from 0mV to -50mV only increases the velocity of the dissolving grain contact by a factor ≈ 2. This is due to the last term in equation [6] $\frac{m_{Na^+}^{0.331}}{a_{H^+}^{0.441}}$. This term reduces the effect of the factor 50 increase in cation concentration near the grain contact due to a decrease in surface potential of -50mV seen in figure 9 to $50^{0.331} = 3.65$. An additional effect of this term is the much larger difference between 0 and 5 mMol cation concentrations and 5 and 30 mMol cation concentration although the absolute difference in concentration is smaller. This can be explained by the $a_{H^+}^{0.441}$ in the term where $a_{H^+} = 1 \cdot 10^{-9}$, the effect of a pH of 9 is an increase in the k^+ value since there is a division by a number < 1. When $m_{Na^+} = 0$ the pH or a_{H^+} no longer has an effect on k^+ since $\frac{0}{a_{H^+}} = 0$. Saturation of the cation sites near the quartz surface at $m_{Na^+} = 50mMol$ Dove et al. (2005) also dampens the effect of lowering the surface potential of the quartz grain contact. To gain full effect of the factor 50 increase in cations due to mica presence, the bulk concentration of cations has to be $\leq 1mMol$.

The optical observations of the grains showed no difference before and after the experiments as can be seen in figure 16. This means the maximum dissolution velocity found in Kristiansen et al. (2011) of $1.4 \cdot 10^{-13}$ meters per second is not representative for the experiments conducted. Since increase in area of the top of the grain if these velocities were true (figure 7) would be visible with an optical microscope. The velocities from the theoretical model are between $\approx 2 \cdot 10^{-15} m/s$ and $\approx 2 \cdot 10^{-20} m/s$. Where in the case of $\approx 2 \cdot 10^{-15} m/s$ the area radius would increase to $2\mu m$ instead of the $14\mu m$ after a month for the velocity of Kristiansen et al. (2011). Free dissolution in water at 25 ° C results in a Δh of 0.0137 $\AA$ per month Tester et al. (1994) which is equal to a velocity of $5.2 \cdot 10^{-}19 m/s$ and 25 faster than the dissolution velocity our model finds for the slowest dissolution at room temperature and no additional driving forces. At these extremely slow dissolution velocities, no dissolution features are expected to be found. We did however find dissolution features in experiment 1 and 2, which contradicts our theoretical model and observations from Tester et al. (1994) unless an additional driving force is added for quartz dissolution at a mica-quartz interface.

Our experiments show evidence for quartz dissolution in 8 out of 10 experimental setups in the form of the presence of etch pits that are visible on the AFM-images after the experiments concluded. No AFM-images before the experiments started showed any evidence of etch pits. After the experiments concluded only experiments 6 and 7 did not show any etch pits, these are two of the three experimental setups with a quartz-quartz contact at low normal grain contact stresses of 0.5 MPa. The other experiment with similar conditions is experiment 8 which has a higher cation concentration (30 mM Ca^{2+}) compared to experiment 6 (0 mM Ca^{2+}) and 7 (5 mM Ca^{2+}). Experiment 6 is the experiment where the lowest dissolving grain contact velocities (V_c) are to be expected, corresponding to the intersection of $\sigma_n = 0.5MPa$ with the dark blue line in figure 11. Another experiment tied for the lowest V_c with experiment 6 is experiment 1 according to the theoretical model, where the only change is a dissimilar contact with mica instead of quartz. So while the same theoretical V_c is expected only one of the two experiments show evidence of dissolution. Additionally a V_c 75 times higher is expected in experiment 7 compared to experiment 1, where experiment 7 did not show evidence of dissolution and experiment 1 did. There are two main ways to explain the difference in results from the theoretical model to the experimental data. The first way is that the effect of a dissimilar interface is much higher in reality than it is in the theoretical model, resulting in dissolution only occurring at quartz-quartz interfaces when either the normal stress is high (100 MPa) or the cation concentration is high (30 mMol Ca^{2+}). While neither of those factors are necessary for dissolution in the experimental setup to occur on a dissimilar mica-quartz interface. The second explanation is that due to the relative rarity of being able to see etch pits on the AFM-images after the experiments that etch pits did develop on the samples from experiment 6 and 7, but the problem with those etch pits are that they are not measured with the AFM afterwards. The AFM-images of experiments where etch pits are found did not show evidence of etch pits on the majority of AFM-images of the experiment, but only on a select few. On the majority of AFM-images after the experiments concluded the etch pits are not present or obstructed by larger scale asperities ($\geq 100nm$) that are present before the experiments as well. This could be the case for all AFM-images in experiments 6 and 7 after the experiment.

The results of the roughness analysis of the AFM-images are shown in figures 20 and 19. The figures show large average deviations, the two experimental setups with the smallest average deviations compared to the average are experiment 6 and 7. For both these experiments it can be seen that the average roughness shows very little change between before and after the experiment, $< 1\%$ and 7% for experiments 6 and 7 respectively. Where some experiments with relatively large average deviations such as 1 and 8 show relatively large changes of 55% and 36% in average roughness, between before and after. Both experiments with relatively low average deviations (6 and 7) are the experiments where after the experiments there was no evidence of dissolution. There could be two reasons for this, firstly it could show that when there is no dissolution the roughness of the samples remain relatively unchanged. The second reason is that in addition to the absence of images with evidence of dissolution in experiments 6 and 7, there is also an absence of images on the scale that are capable of showing etch pits. This means that the images from after experiment 6 and 7 are all on a more similar scale resulting in a lower average deviation. Overall we think the roughness results are mostly a result of initial geometry present on the grains and the flaws of the AFM on relatively rough and sloped samples, so that makes the second reason for the low average deviation in experiments 6 and 7 more likely than the first.

The hypotheses that are proposed in an earlier section require more experimental evidence to truly confirm the validity of the theoretical model. The main part we can take from the results is that if no dissolution occurred in experiments 6 and 7 and there was dissolution in the other experiments. It could require an additional dependence of the velocity of the dissolving quartz grain contact in the theoretical model on the presence of mica that does not depend on the effect it has on the attraction of additional cations to the quartz contact. This additional effect could be the lowering of the surface potential due to mica proximity of the quartz grain on a boundary that is not experiencing normal stress. This will create an additional potential difference between the stressed boundary and the unstressed boundary leading to a bigger total potential difference and increasing the dissolution rate of the quartz at the stressed boundary resulting in a higher dissolution velocity.

A problem with our theoretical model is that it only looks at the velocity at which the dissolving quartz contact retreats, this velocity is linked to the total compaction of the sandstone. But to look at the total compaction of a sandstone with mica presence, more investigation should be done regarding the dissolution and compaction of the mica grains themselves. This is especially important when the mica make up a significant amount of the total volume of the sandstone.

The main problem with the experimental setup is that the surfaces of grains are highly irregular and that difference in scales at which the features are represented can not be accurately measured on a curved surface using an AFM. The curved surface limits the scan size to a maximum of 9 μm^2, since any larger surfaces will curve down and away from the AFM tip if you start at the top of the sample. An additional problem is that the only clear reference point is the top of the sample found using the optical microscope. This combined with the small scan size makes it impossible to directly relate two scan surfaces from before and after the experiments. This is attempted to be avoided by rigorously scanning the area surrounding the top of the sample. This results in two sets of data from before and after that are scanned in the same area. The idea was that by qualitatively looking at the dissolution features the before and after images could still be compared.

To improve the experimental setup we would suggest not using quartz grains with irregular surfaces, but to instead use flat quartz single crystal surfaces that can be marked with reference points. This will enable direct comparison of surface areas as well as greater scan sizes, due to the AFM tip not being hindered by the curvature of the grain surface. An additional benefit is that the surface scans will probably show asperities on a more similar scale due to the lack of larger asperities on the single crystal quartz compared to quartz grains before the experiments start, which also makes comparison of dissolution features between the different experimental setups easier.

7 Conclusion

Our theoretical model shows both an influence from a contact between two dissimilar surfaces and a contact stress can lead to an increase in dissolution velocity. These effects can be observed simultaneously in natural samples of sandstones. Where both the presence of a dissimilar mica-quartz grain contact and an increase in normal stress across the grain contact lead to an increase in the velocity of the dissolving grain boundary. According to our theoretical model the difference between a quartz-quartz contact and a mica-quartz contact leads to a factor ≈ 2 increase in dissolution velocity of the quartz grain, when 5mM of cations (Na^+ or Ca^{2+})are present in the interstitial water. Increasing the normal stress across the grain contact from 0.5 MPa to 100 MPa can lead to a factor ≈ 1200 increase in dissolution velocity. Dissolution features are found in our experiments on quartz grain surfaces where low dissolution velocities were predicted by the model, as long as in the experiment a mica-quartz contact is present or the cation concentration in the bulk fluid was 30 mM. Roughness analysis with the atomic force microscope (AFM) of the quartz grain surfaces showed no relation to theoretically predicted dissolution velocities. The roughness analysis showed a relation to the observed dissolution features on the quartz grain surfaces. This relation might however be caused by inherent flaws of using an AFM on quartz grain samples with a lot of initial geometry on both the μm-scale and nm-scale. Additional research needs to be done on smoother single crystal quartz surfaces to reach more conclusive experimental results.

8 Bibliography

Binnig, G., Quate, C. F., and Gerber, C. (1986). Atomic force microscope. *Physical review letters*, 56(9):930.

Brzesowsky, R. H., Spiers, C. J., Peach, C. J., and Hangx, S. J. T. (2011). Failure behavior of single sand grains: Theory versus experiment. *Journal of Geophysical Research: Solid Earth*, 116(B6):n/a–n/a. B06205.

Dove, P. M., Han, N., and De Yoreo, J. J. (2005). Mechanisms of classical crystal growth theory explain quartz and silicate dissolution behavior. *Proceedings of the National Academy of Sciences*, 102(43):15357–15362.

Dove, P. M. and Nix, C. J. (1997). The influence of the alkaline earth cations, magnesium, calcium, and barium on the dissolution kinetics of quartz. *Geochimica et Cosmochimica Acta*, 61(16):3329–3340.

Greene, G. W., Kristiansen, K., Meyer, E. E., Boles, J. R., and Israelachvili, J. N. (2009). Role of electrochemical reactions in pressure solution. *Geochimica et Cosmochimica Acta*, 73(10):2862–2874.

Heald, M. and Baker, G. (1977). Diagenesis of the mt. simon and rose run sandstones in western west virginia and southern ohio. *Journal of Sedimentary Research*, 47(1).

Heald, M. T. (1956). Cementation of simpson and st. peter sandstones in parts of oklahoma, arkansas, and missouri. *The Journal of Geology*, pages 16–30.

Israelachvili, J. N., Kristiansen, K., Gebbie, M. A., Lee, D. W., Donaldson Jr, S. H., Das, S., Rapp, M. V., Banquy, X., Valtiner, M., and Yu, J. (2013). The intersection of interfacial forces and electrochemical reactions. *The Journal of Physical Chemistry B*, 117(51):16369–16387.

Kristiansen, K., Valtiner, M., Greene, G. W., Boles, J. R., and Israelachvili, J. N. (2011). Pressure solution–the importance of the electrochemical surface potentials. *Geochimica et Cosmochimica Acta*, 75(22):6882–6892.

Niemeijer, A. and Spiers, C. (2002). Compaction creep of quartz-muscovite mixtures at 500 c: Preliminary results on the influence of muscovite on pressure solution. *Geological Society, London, Special Publications*, 200(1):61–71.

Niemeijer, A., Spiers, C., and Bos, B. (2002). Compaction creep of quartz sand at 400–600 c: Experimental evidence for dissolution-controlled pressure solution. *Earth and Planetary Science Letters*, 195(3):261–275.

Pluymakers, A. and Spiers, C. (2015). Compaction creep of simulated anhydrite fault gouge by pressure solution: theory v. experiments and implications for fault sealing. *Geological Society, London, Special Publications*, 409(1):107–124.

Rimstidt, J. D. (2015). Rate equations for sodium catalyzed quartz dissolution. *Geochimica et Cosmochimica Acta*, 167:195–204.

Robinson, A. and Gluyas, J. (1992). Model calculations of loss of porosity in sandstones as a result of compaction and quartz cementation. *Marine and Petroleum Geology*, 9(3):319–323.

Sibley, D. F. and Blatt, H. (1976). Intergranular pressure solution and cementation of the tuscarora orthoquartzite. *Journal of Sedimentary Research*, 46(4).

Simmons, G. and Wang, H. (1971). Single crystal constants and calculated aggregate properties: A handbook. *MTI Press, Cambridge*.

Tada, R. and Siever, R. (1989). Pressure solution during diagenesis. *Annual Review of Earth and Planetary Sciences*, 17:89.

Tester, J. W., Worley, W. G., Robinson, B. A., Grigsby, C. O., and Feerer, J. L. (1994). Correlating quartz dissolution kinetics in pure water from 25 to 625 c. *Geochimica et Cosmochimica Acta*, 58(11):2407–2420.

Thomson, A. (1959). Pressure solution and porosity.

van Noort, R. and Spiers, C. J. (2009). Kinetic effects of microscale plasticity at grain boundaries during pressure solution. *Journal of Geophysical Research: Solid Earth*, 114(B3).

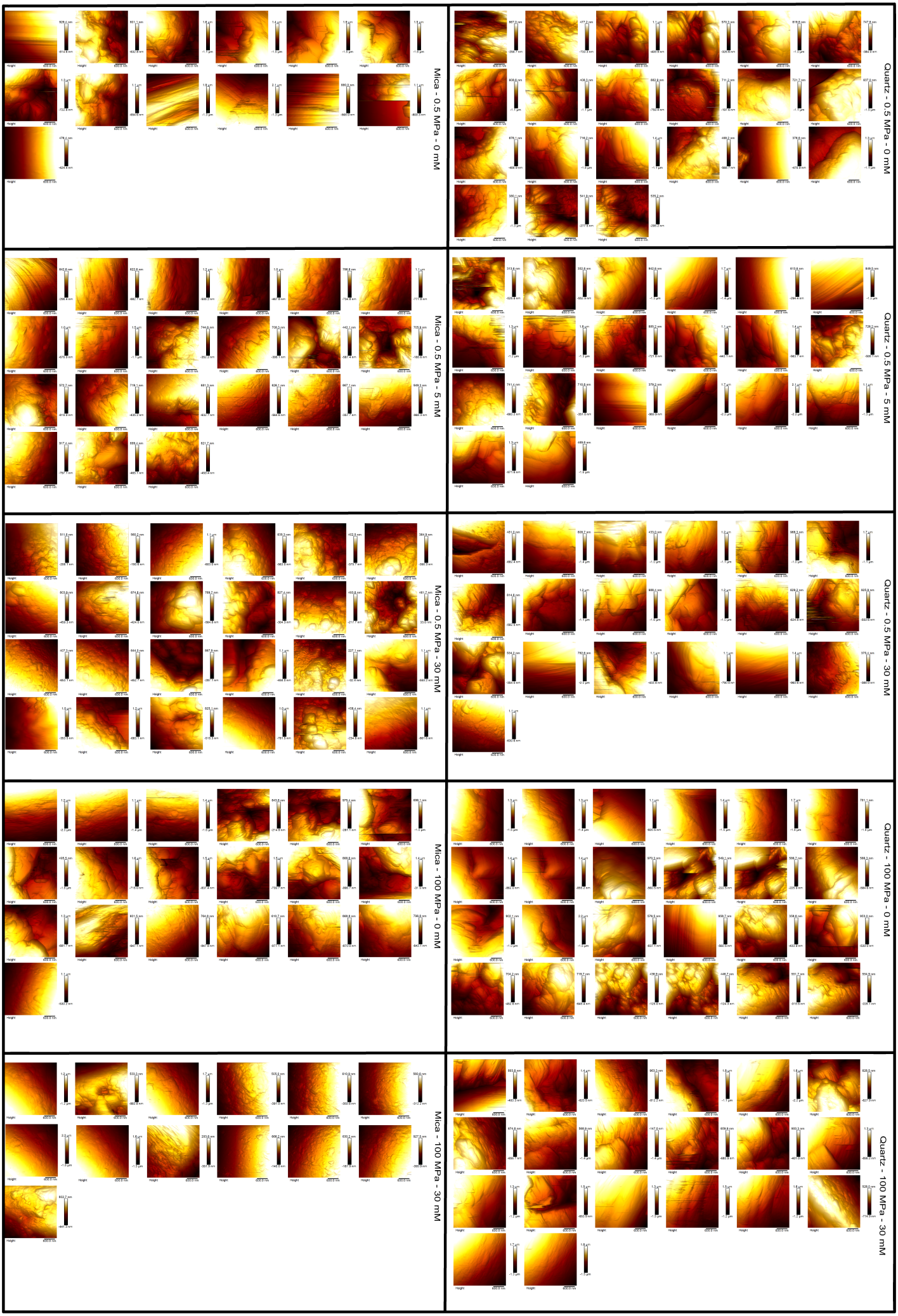
Mica - 0.5 MPa - 0 mM
Quartz - 0.5 MPa - 0 mM
Mica - 0.5 MPa - 5 mM
Quartz - 0.5 MPa - 5 mM
Mica - 0.5 MPa - 30 mM
Quartz - 0.5 MPa - 30 mM
Mica - 100 MPa - 0 mM
Quartz - 100 MPa - 0 mM
Mica - 100 MPa - 30 mM
Quartz - 100 MPa - 30 mM

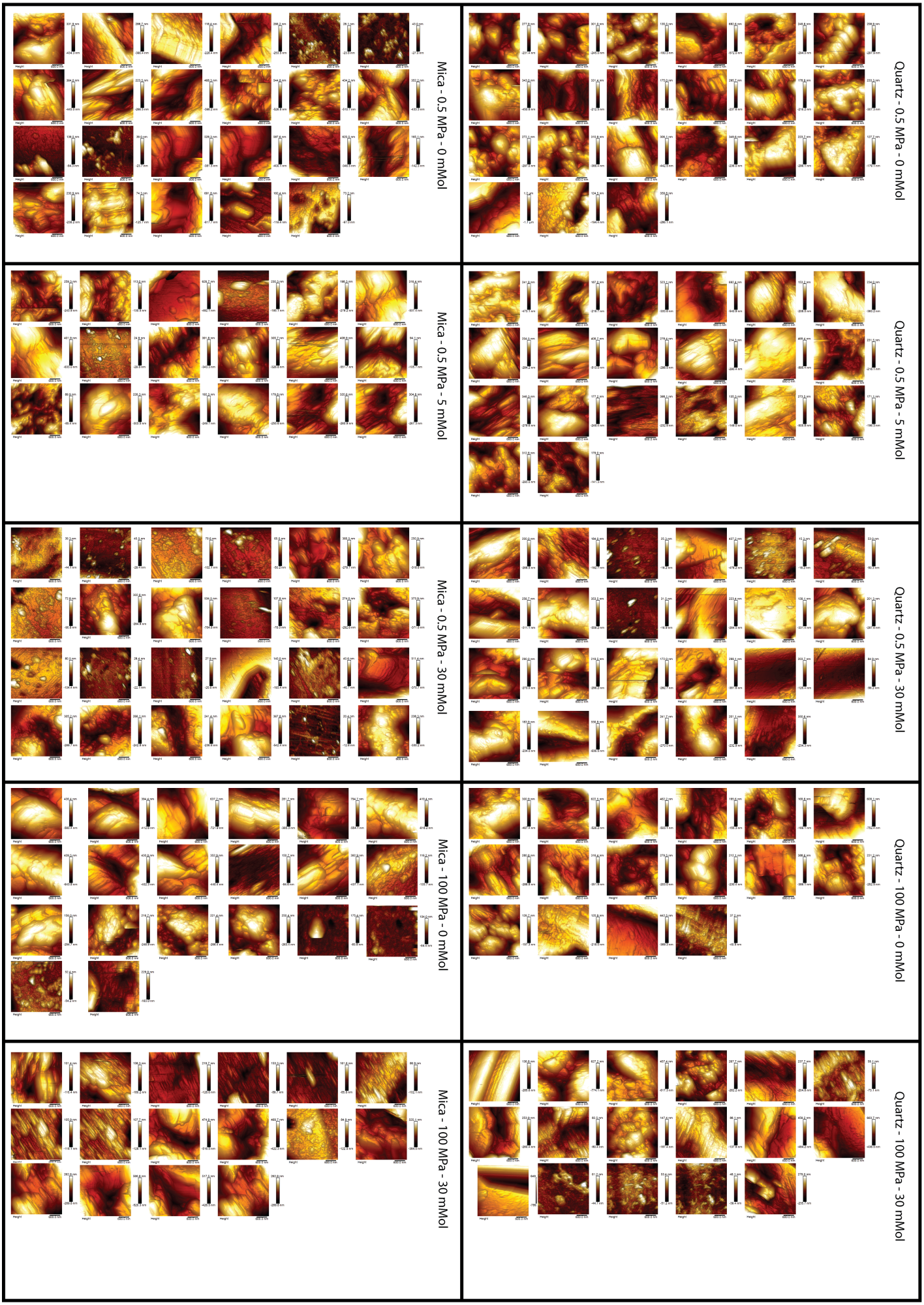
Mica - 0.5 MPa - 0 mMol
Quartz - 0.5 MPa - 0 mMol
Mica - 0.5 MPa - 5 mMol
Quartz - 0.5 MPa - 5 mMol
Mica - 0.5 MPa - 30 mMol
Quartz - 0.5 MPa - 30 mMol
Mica - 100 MPa - 0 mMol
Quartz - 100 MPa - 0 mMol
Mica - 100 MPa - 30 mMol
Quartz - 100 MPa - 30 mMol